

Simultaneous Spin-Charge Relaxation in Double Quantum Dots

V. Srinivasa,^{1,*} K. C. Nowack,² M. Shafiei,² L. M. K. Vandersypen,² and J. M. Taylor¹

¹*Joint Quantum Institute, University of Maryland, College Park,
MD 20742 and National Institute of Standards and Technology, Gaithersburg, MD 20899*

²*Kavli Institute of Nanoscience, TU Delft, Lorentzweg 1, 2628CJ Delft, the Netherlands*

We investigate phonon-induced spin and charge relaxation mediated by spin-orbit and hyperfine interactions for a single electron confined within a double quantum dot. A simple toy model incorporating both direct decay to the ground state of the double dot and indirect decay via an intermediate excited state yields an electron spin relaxation rate that varies non-monotonically with the detuning between the dots. We confirm this model with experiments performed on a GaAs double dot, demonstrating that the relaxation rate exhibits the expected detuning dependence and can be electrically tuned over several orders of magnitude. Our analysis suggests that spin-orbit mediated relaxation via phonons serves as the dominant mechanism through which the double-dot electron spin-flip rate varies with detuning.

Controlling individual spins is central to spin-based quantum information processing [1–3] and also enables precision metrology [4, 5]. While rapid control can be achieved by coupling the spins of electrons in semiconductor quantum dots [1, 2] to electric fields via the electronic charge state [3, 6–14], spin-charge coupling also leads to relaxation of the spins through fluctuations in their electrostatic environment. Phonons serve as an inherent source of fluctuating electric fields in quantum dots [2] and give rise to both charge and spin relaxation through the electron-phonon interaction. In GaAs quantum dots, the direct coupling of spin to the strain field produced by phonons is expected to be inefficient [15, 16]. The dominant mechanisms of phonon-induced spin relaxation are therefore indirect and involve spin-charge coupling due to primarily spin-orbit [15–21] and hyperfine [22–27] interactions. Confining an electron within a double quantum dot (DQD) provides a high degree of control over the charge state [28–31], so that relaxation rates can be varied over multiple orders of magnitude by adjusting the energy level detuning between the dots [25, 32–35].

Here, we investigate the interplay of spin and charge relaxation via phonons for a single electron confined to a DQD in the presence of spin-orbit and hyperfine interactions. We present a simple model together with measurements of the electron spin relaxation rate in a GaAs DQD, both of which yield a non-monotonic dependence on the detuning between the dots (see Fig. 3). The experiments provide confirmation of the model and demonstrate the existence of spin “hot spot” features [18–20, 36, 37] at nonzero values of detuning, where relaxation is enhanced by several orders of magnitude. The opposite behavior is observed at zero detuning, where the spin-flip rate exhibits a local minimum. Theoretically, spin hot spots are predicted to occur due to the complete mixing of spin and orbital states at avoided energy crossings associated with spin-orbit coupling [18, 19, 36]. From a practical standpoint, adjusting the detuning to these points represents a potential method for rapid all-electrical spin initialization.

We describe a single electron confined within a DQD (Fig. 1) using a toy model that includes only the lowest-energy orbital level of each dot. This two-level approximation [28] enables the charge degrees of freedom to be represented by the Pauli matrices $\sigma_x, \sigma_y, \sigma_z$ in the basis $\{|L\rangle, |R\rangle\}$, where $|L\rangle$ ($|R\rangle$) denotes an electron in the left (right) quantum dot and $\sigma_z \equiv |L\rangle\langle L| - |R\rangle\langle R|$. We can then express the Hamiltonian of the system as

$$H_d = H_0 + H_{so} + H_{nuc}, \quad (1)$$

$$H_0 = \frac{\epsilon}{2} \sigma_z - t \sigma_x - \Omega_z S_z, \quad (2)$$

$$H_{so} = \mathbf{K}_{so} \cdot \mathbf{S} \sigma_y, \quad (3)$$

$$H_{nuc} = \mathbf{K}_{nuc} \cdot \mathbf{S} \sigma_z. \quad (4)$$

The first two terms in H_0 [Eq. (2)] specify the purely orbital part $H_{orb} \equiv (\epsilon/2) \sigma_z - t \sigma_x$ of the electronic Hamiltonian in terms of the energy level detuning ϵ and the

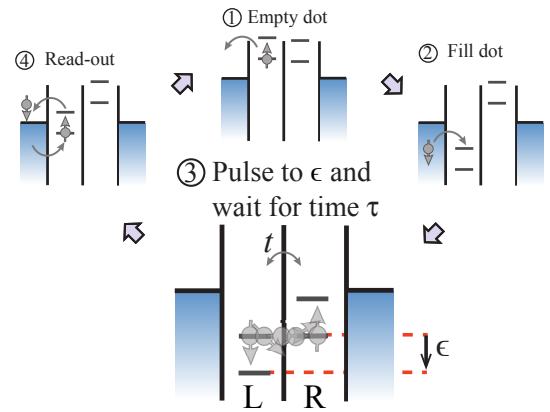


Figure 1: Electrochemical potential diagrams for a double quantum dot (DQD), illustrating the measurement cycle used to obtain the experimental spin relaxation rate (see main text). Varying the detuning ϵ between the left (L) and right (R) dots while keeping the tunnel coupling t fixed (stage 3) tunes the relative energies of the charge states. Tunneling of the electron between the dots is accompanied by spin rotation.

tunnel coupling t between the two dots (Fig. 1). Diagonalization of H_{orb} yields the eigenstates

$$\begin{aligned} |+\rangle &\equiv \cos \frac{\phi}{2} |L\rangle - \sin \frac{\phi}{2} |R\rangle, \\ |-\rangle &\equiv \sin \frac{\phi}{2} |L\rangle + \cos \frac{\phi}{2} |R\rangle, \end{aligned} \quad (5)$$

where ϕ varies with ϵ and t according to $\tan \phi = 2t/\epsilon$. The corresponding eigenvalues are separated in energy by a gap $\Delta = E_+ - E_- = \sqrt{\epsilon^2 + 4t^2}$ [see also Fig. 2(a)].

Spin dependence is introduced into the Hamiltonian via the last term in H_0 , together with H_{so} and H_{nuc} [see Eqs. (2)-(4)], where the vector of electron spin operators is denoted by $\mathbf{S} = (S_x, S_y, S_z)$. The term H_{so} describes spin-orbit coupling which is linear in the electron momentum \mathbf{p} . The general form given in Eq. (3) takes into account both the Rashba [38, 39] and the linear Dresselhaus [40] forms of spin-orbit interaction, with strengths and orientations that are specified by the vector $\mathbf{K}_{\text{so}} \equiv (r, s, q)$. Note that H_{so} acts as σ_y within the orbital subspace, which follows from parity selection rules for the matrix elements of \mathbf{p} in the basis $\{|L\rangle, |R\rangle\}$. Thus, H_{so} describes tunneling between the dots accompanied by a spin flip (Fig. 1) [13].

The remaining spin-dependent terms in H_d represent forms of the Zeeman interaction that are distinguished by their action within the orbital subspace. The final term in H_0 represents the coupling of the electron spin to a magnetic field of strength $B = \Omega_z/|g|\mu_B$ that is uniform over the two dots, where g is the electron g-factor and μ_B is the Bohr magneton. The vector $\mathbf{K}_{\text{nuc}} \equiv (u, v, w)$ in H_{nuc} specifies the strength and orientation of a magnetic field gradient across the two dots. H_{nuc} acts as σ_z within the orbital subspace. For GaAs quantum dots, H_{nuc} can be used to model the hyperfine interaction between the electron spin and the ensemble of nuclear spins with which the electron wavefunction overlaps. The associated intrinsic magnetic field gradient is assumed to originate from an effective nuclear field \mathbf{B}_{nuc} with a random, spatially-varying orientation described by a Gaussian distribution and magnitude B_{nuc} given by the root-mean-square (rms) value [23-25, 27, 41].

Figure 1 illustrates the scheme used for the measurement of the spin relaxation rate. The experimental setup is described in [42]. In the first step of the measurement cycle, a single electron spin is initialized by emptying the DQD and then letting a single electron tunnel into the left dot far from the degeneracy of $|L\rangle$ and $|R\rangle$. The electron spin is randomly up or down. Next, a voltage pulse adjusts the electrochemical potential of the right dot to tune the detuning closer to the degeneracy to a value ϵ for a wait time τ . After the wait time, the electrochemical potential is pulsed back and the spin of the electron is read out using energy-selective spin-to-charge conversion [43]. This cycle is repeated for a given ϵ and τ to obtain an average spin-down probability at the end of the cycle.

For each series of measurements as a function of τ at a fixed ϵ , the amount of detected spin-down is fitted with an exponential decay, from which the spin-relaxation rate at each ϵ is obtained as shown in Fig. 3.

The variation of the measured spin relaxation rate with detuning can be understood in terms of the spectrum for the one-electron double dot. Figure 2(a) shows an example spectrum for H_d [Eq. (1)] as a function of detuning. In Fig. 2 and throughout the present work, we consider the limit $t \ll \Omega_z$ which corresponds to the measurements described above (see [42]). The notation \uparrow, \downarrow used to label the states in the figure refers to the components of spin along the quantization axis defined by the external magnetic field. In accordance with the experiment [42, 44], we choose this field to be in the plane of the quantum dots and parallel to the double-dot axis. The in-plane crystal lattice orientation characterizing the spin-orbit interaction [Eq. (3)] is parametrized by an angle θ relative to this axis. Of particular consequence for the present work is the fact that H_{so} gives rise to avoided crossings in the spectrum at $\epsilon \approx \pm \Omega_z$, where maximal coupling of the states $|+, \uparrow\rangle$ and $|-, \downarrow\rangle$ occurs and leads to the complete mixing of orbital and spin degrees of freedom. These finite values of ϵ correspond to spin “hot spots” [18-20, 36, 37] and are associated with enhanced spin relaxation rates, as is shown below.

Including coupling to phonons in the description of the single-electron double-dot system leads to the Hamiltonian $H = H_d + H_{\text{ep}}$, where

$$\begin{aligned} H_{\text{ep}} = \sum_{\nu, \mathbf{k}} & \sqrt{\frac{\hbar}{2\rho_0 V_0 c_\nu k}} (k\beta_l \delta_{\nu, l} - i\Xi) \\ & \times \left(a_{\nu, \mathbf{k}} + a_{\nu, -\mathbf{k}}^\dagger \right) e^{i\mathbf{k} \cdot \mathbf{r}} \end{aligned} \quad (6)$$

is the electron-phonon interaction [45], expressed in terms of the mass density ρ_0 , the volume V_0 , the phonon speeds c_ν , the deformation potential β_l , and the piezoelectric constant Ξ . The operator $a_{\nu, \mathbf{k}}^\dagger$ ($a_{\nu, \mathbf{k}}$) creates (annihilates) a phonon with wavevector \mathbf{k} and polarization ν [the sum over ν is taken over one longitudinal (l) mode and two transverse (t) modes], and $\delta_{\nu, l}$ is the Kronecker delta function. Fermi’s golden rule for the rate Γ of phonon-induced relaxation of the electron from state $|i\rangle$ to state $|f\rangle$ of the double dot gives $\Gamma \sim |\langle f | H_{\text{ep}} | i \rangle|^2 \rho(\Delta_d)$, where $\rho(\Delta_d)$ is the phonon density of states evaluated at the gap Δ_d between levels i and f that determines the energy of the emitted phonon.

We first consider a qualitative model for Γ , where we estimate the transition matrix element $\langle f | e^{i\mathbf{k} \cdot \mathbf{r}} | i \rangle$ (see [42]) by writing $e^{i\mathbf{k} \cdot \mathbf{r}} \approx 1 + i\mathbf{k} \cdot \mathbf{r}$ and determining the corresponding matrix element of the dipole operator $\mathbf{d} = -e\mathbf{r}$ (here, e denotes the magnitude of the electron charge). To evaluate dipole matrix elements, we define Gaussian wavefunctions $\psi_{L(R)}(\mathbf{r}) \equiv \langle \mathbf{r} | L(R) \rangle$ which are shifted along the dot axis by $\pm a/2$ for the left-localized and right-

localized orbital states. While ψ_L and ψ_R are not orthogonal, their overlap is small. We neglect corrections due to this overlap in our calculations. Using these wavefunctions, we find $\mathbf{d} = D\hat{z}$ with $D = (ea/2)\sigma_z$. The qualitative form of the relaxation rate can then be approximated by $\Gamma \sim |d|^2 F(\Delta_d)$, where d denotes the first-order term of $\langle f|D|i\rangle$ and $F(\Delta_d)$ represents the dependence of the rate on the gap energy Δ_d (see [42] for more details).

To identify the states of the double dot between which phonon-induced relaxation occurs, we treat $V \equiv H_{\text{so}} + H_{\text{nuc}}$ [Eqs. (3) and (4)] as a perturbation with respect to H_0 [Eq. (2)] and use nondegenerate perturbation theory (which is valid away from $\epsilon \approx \pm\Omega_z$) to find the first-order corrections to the energies and eigenstates of H_0 . We denote the corrected states by $\{|\tilde{-}, \uparrow\rangle, |\tilde{-}, \downarrow\rangle, |\tilde{+}, \uparrow\rangle, |\tilde{+}, \downarrow\rangle\}$ and consider relaxation of the electron spin from the excited state $|\tilde{-}, \downarrow\rangle$ to the ground state $|\tilde{-}, \uparrow\rangle$ of the DQD [see Fig. 2(a)], which can occur directly as well as indirectly via the excited state $|\tilde{+}, \uparrow\rangle$. Away from the avoided crossing points, we note that $|\tilde{+}, \uparrow\rangle \approx |\tilde{+}, \uparrow\rangle$ and $|\tilde{-}, \uparrow\rangle \approx |\tilde{-}, \uparrow\rangle$. The state $|\tilde{+}, \uparrow\rangle$ therefore relaxes rapidly to $|\tilde{-}, \uparrow\rangle$, as effectively only orbital decay is involved and no spin flip is required in this second step [46]. In the following, we assume that this charge relaxation is instantaneous compared to the spin relaxation and use the dipole matrix element for $|\tilde{-}, \downarrow\rangle \rightarrow |\tilde{+}, \uparrow\rangle$ to describe the full indirect transition.

We approximate the relaxation rates Γ_b and Γ_e [Fig. 2(a)] in the presence of both H_{so} and H_{nuc} by calculating the first-order terms d_b and d_e of the dipole matrix elements $\langle \tilde{-}, \uparrow | D | \tilde{-}, \downarrow \rangle$ and $\langle \tilde{+}, \uparrow | D | \tilde{-}, \downarrow \rangle$, respectively. These terms are functions of the spin-flipping components r , s , u , and v in Eqs. (3) and (4). Averaging over the nuclear field distribution [23–25, 27]

$$P(\mathbf{K}_{\text{nuc}}) = \frac{1}{(2\pi b_{\text{nuc}}^2)^{3/2}} \exp\left(-\frac{|\mathbf{K}_{\text{nuc}}|^2}{2b_{\text{nuc}}^2}\right), \quad (7)$$

where $b_{\text{nuc}} \equiv |g|\mu_B B_{\text{nuc}} = \sqrt{\langle |\mathbf{K}_{\text{nuc}}|^2 \rangle}/3$, gives $\langle u \rangle = \langle v \rangle = 0$ and $\langle u^2 \rangle = \langle v^2 \rangle = b_{\text{nuc}}^2$. We thus find

$$\langle |d_b|^2 \rangle = \left[\frac{ea}{2} \left(\frac{2t}{\Delta} \right) \frac{\Omega_z}{(\Delta - \Omega_z)(\Delta + \Omega_z)} \right]^2 \chi, \quad (8)$$

$$\langle |d_e|^2 \rangle = \left[\frac{ea}{2} \left(\frac{\epsilon}{\Delta} \right) \frac{1}{\Delta - \Omega_z} \right]^2 \chi, \quad (9)$$

$$\chi \equiv \left[r^2 + s^2 + \left(\frac{2t}{\Omega_z} \right)^2 (2b_{\text{nuc}}^2) \right].$$

These expressions are plotted in Fig. 2(b). Note that both Eqs. (8) and (9) are undefined at the avoided crossing points in Fig. 2(a), where $\Delta = \Omega_z$. Thus, the curves shown in Fig. 2(b) are valid only away from these points (i.e., where nondegenerate perturbation theory is a reasonable approximation). Both $\langle |d_b|^2 \rangle$ and $\langle |d_e|^2 \rangle$ are only

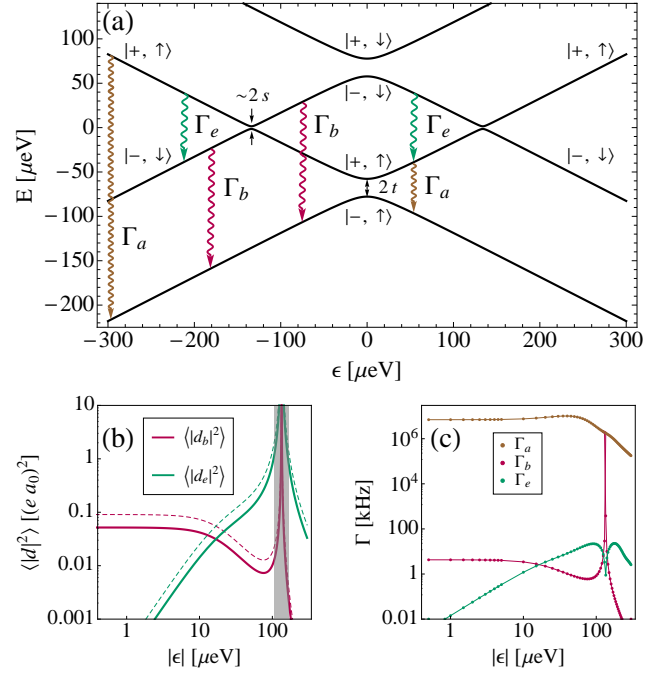


Figure 2: (a) Spectrum of H_d [Eq. (1)] as a function of detuning ϵ for the case $t \ll \Omega_z$, in the presence of spin-orbit coupling ($\mathbf{K}_{\text{so}} \neq \mathbf{0}$, $\mathbf{K}_{\text{nuc}} = \mathbf{0}$). Correspondence with the eigenstates of H_0 [Eqs. (2) and (5)] is indicated for relevant regions of the spectrum. Avoided crossings due to spin-orbit coupling occur at $\epsilon \approx \pm\Omega_z$. The spectrum shown corresponds to $t = 10 \mu\text{eV}$ [42], $B = 6.5 \text{ T}$ [42, 44], the dot size $\sigma = 15 \text{ nm}$ and interdot separation $a = 110 \text{ nm}$, the GaAs effective mass $m^* = 0.067m_e$ (where m_e is the free-electron mass) and g-factor $g = 0.36$, the Rashba and linear Dresselhaus spin-orbit strengths $\alpha_0 = 3.3 \times 10^{-12} \text{ eV}\cdot\text{m}$ and $\beta_0 = 4.5 \times 10^{-12} \text{ eV}\cdot\text{m}$, respectively, and $\theta = \pi/8$. The values of α_0 , β_0 , and θ are used to determine $\mathbf{K}_{\text{so}} = (r, s, q)$. (b) Dipole-dependent factors $\langle |d_b|^2 \rangle$ and $\langle |d_e|^2 \rangle$ [Eqs. (8) and (9)] used to qualitatively model the relaxation rates Γ_b and Γ_e in (a), as a function of detuning for $B_{\text{nuc}} = 0$ (solid lines) and $B_{\text{nuc}} = 3 \text{ mT}$ (dotted lines), with $\alpha_0 = 3.3 \times 10^{-14} \text{ eV}\cdot\text{m}$ and $\beta_0 = 4.5 \times 10^{-14} \text{ eV}\cdot\text{m}$. All other parameters are identical to those used in (a). Units for the dipole are given in terms of the Bohr radius a_0 . The dipole moment is not valid in the shaded region. (c) Relaxation rates Γ_a , Γ_b , and Γ_e as a function of detuning. The rates are calculated using $\rho_0 = 5.3 \times 10^3 \text{ kg/m}^3$, $c_l = 5.3 \times 10^3 \text{ m/s}$, $c_t = 2.5 \times 10^3 \text{ m/s}$, $\beta_l = 7.0 \text{ eV}$, and $\Xi = 1.4 \times 10^9 \text{ eV/m}$ [20], together with the parameter values used in (b). Lines are guides to the eye.

slightly modified by the coupling of the electron spin to an effective nuclear field of rms strength $B_{\text{nuc}} = 3 \text{ mT}$ [25], as expected from Eqs. (8) and (9) in which the nuclear field term is scaled with respect to the spin-orbit terms by a factor $(2t/\Omega_z)^2 \ll 1$ [13]. Saturation of $\langle |d_b|^2 \rangle$ occurs at zero detuning for both the $B_{\text{nuc}} = 0$ and the $B_{\text{nuc}} = 3 \text{ mT}$ cases. On the other hand, $\langle |d_e|^2 \rangle$ vanishes at $\epsilon = 0$ regardless of the value of B_{nuc} . As the experimental relaxation rate contains a local minimum at zero

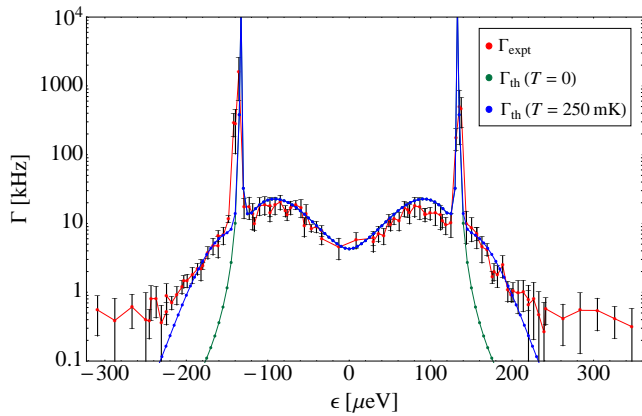


Figure 3: Experimental detuning-dependent single-spin relaxation rate (Γ_{expt}) and comparison with the toy model described in the present work (Γ_{th}) for both zero and finite temperature. Error bars depict 90% confidence intervals for the data. The parameter values used to calculate Γ_{th} are the same as those used in (b) and (c) of Fig. 2.

detuning (see Fig. 3), the present analysis suggests that the direct transition $|\downarrow, \downarrow\rangle \rightarrow |\downarrow, \uparrow\rangle$ alone does not account for the observed spin relaxation and that indirect relaxation via the excited state $|\uparrow, \uparrow\rangle$ potentially plays a significant role in the spin-flip rate. The relative contributions of the direct and indirect transitions to the overall rate are explored in [42].

To compare our theoretical predictions more directly with the experimental results, we carry out the full calculation of the relaxation rates for both direct and indirect transitions to the ground state by applying Fermi's golden rule to relaxation induced by H_{ep} [Eq. (6)]. Details are given in the Supplemental Material [42]. We set $\mathbf{K}_{\text{nuc}} = 0$ for simplicity, as the preceding analysis based on dipole matrix elements suggests that the hyperfine term H_{nuc} represents only a small correction to the decay rate [see Eqs. (8), (9) and Fig. 2(b)]. Application of a Schrieffer-Wolff transformation [47] enables diagonalization of the full double-dot Hamiltonian H_d for all ϵ , including the avoided crossing points $\epsilon \approx \pm\Omega_z$, and the eigenstates of H_d are used to calculate the relaxation rates via Eqs. (S1)-(S3) [42].

Relevant portions of the curves for the decay rates Γ_{21} , Γ_{31} , and Γ_{32} (where we number the levels according to their energy eigenvalues and use Γ_{if} to denote the rate of relaxation from level i to level f) are plotted together in Fig. 2(c). The rate Γ_a is associated with mainly charge relaxation and is given by Γ_{21} (Γ_{31}) for $|\epsilon| \lesssim \Omega_z$ ($|\epsilon| \gtrsim \Omega_z$), while Γ_b is associated with mainly spin relaxation and is given by Γ_{31} (Γ_{21}) for $|\epsilon| \lesssim \Omega_z$ ($|\epsilon| \gtrsim \Omega_z$). The rate Γ_e corresponds to a combination of spin and charge relaxation and is given by Γ_{32} for all $|\epsilon|$. Note that $\Gamma_a \gg \Gamma_e$, which is consistent with our prior assumption that the effective rate for indirect relaxation to the ground

state is determined by Γ_e .

For $|\epsilon| \lesssim \Omega_z$, indirect spin relaxation occurs by a transition to the lower-energy intermediate state via phonon emission [Fig. 2(a)]. On the other hand, the indirect transition for $|\epsilon| \gtrsim \Omega_z$ requires phonon absorption in order to excite the electron to the higher-energy intermediate state. Using the Einstein coefficients and the Bose-Einstein distribution $\langle n \rangle = 1/[\exp(\Delta_d/k_B T) - 1]$ (where k_B is the Boltzmann constant and T is the temperature) to express the rates of spontaneous emission, stimulated emission, and absorption associated with the lowest three double-dot levels in Fig. 2(a) in terms of Γ_a , Γ_b , and Γ_e [32], we take the full theoretical detuning-dependent spin relaxation rate Γ_{th} to be given by $\Gamma_b + \Gamma_e$ for $|\epsilon| \lesssim \Omega_z$ and by $\Gamma_b + \Gamma_e \langle n \rangle / (\langle n \rangle + 1)$ for $|\epsilon| \gtrsim \Omega_z$. This rate is plotted together with the zero-temperature limit of the model and the measured rate Γ_{expt} in Fig. 3 for $T = 250$ mK [42, 44]. At the avoided crossings associated with spin-orbit coupling ($\epsilon \approx \pm\Omega_z$), we find peaks in Γ_{th} that resemble the spin hot spot peaks observed experimentally. The zero-detuning minimum found in the measurements appears in both the zero- and the finite-temperature models. In addition, close qualitative agreement between the finite-temperature model and experiment is observed for a wide range of detuning values. While limitations of our theoretical description arise from the two-level approximation we use for the orbital states, we have nevertheless shown that several characteristic features present in the measured detuning dependence of the double-dot spin relaxation rate can be understood within this simple model.

The results of the present work therefore suggest that, in accordance with the case of single lateral GaAs quantum dots [21], the observed variation of the spin relaxation rate with detuning in double dots is dominated by spin-orbit mediated electron-phonon coupling. The spin-orbit interaction may thus provide the key to rapid all-electrical initialization of single spins.

Note added. During the preparation of this manuscript, we became aware of a recent experimental observation of a spin hot spot in a Si quantum dot [48].

We thank N. M. Zimmerman, M. D. Stiles, and P. Stano for helpful comments. Research was supported by DARPA MTO, the Office of the Director of National Intelligence, Intelligence Advanced Research Projects Activity (IARPA), through the Army Research Office (Grant W911NF-12-1-0354), SOLID (EU), and an ERC Starting Grant.

* Electronic address: vsriniv@umd.edu

- [1] D. Loss and D. P. DiVincenzo, Phys. Rev. A **57**, 120 (1998).
- [2] R. Hanson, L. P. Kouwenhoven, J. R. Petta, S. Tarucha, and L. M. K. Vandersypen, Rev. Mod. Phys. **79**, 1217

- (2007).
- [3] R. Hanson and D. D. Awschalom, *Nature* **453**, 1043 (2008).
 - [4] J. M. Taylor, P. Cappellaro, L. Childress, L. Jiang, D. Budker, P. R. Hemmer, A. Yacoby, R. Walsworth, and M. D. Lukin, *Nature Phys.* **4**, 810 (2008).
 - [5] F. Dolde, H. Fedder, M. W. Doherty, T. Nobauer, F. Rempp, G. Balasubramanian, T. Wolf, F. Reinhard, L. C. L. Hollenberg, F. Jelezko, and J. Wrachtrup, *Nature Phys.* **7**, 459 (2011).
 - [6] Y. Kato, R. C. Myers, D. C. Driscoll, A. C. Gossard, J. Levy, and D. D. Awschalom, *Science* **299**, 1201 (2003).
 - [7] E. I. Rashba and A. L. Efros, *Phys. Rev. Lett.* **91**, 126405 (2003).
 - [8] J. M. Taylor, H. A. Engel, W. Dur, A. Yacoby, C. M. Marcus, P. Zoller, and M. D. Lukin, *Nature Phys.* **1**, 177 (2005).
 - [9] Y. Tokura, W. G. van der Wiel, T. Obata, and S. Tarucha, *Phys. Rev. Lett.* **96**, 047202 (2006).
 - [10] K. C. Nowack, F. H. L. Koppens, Y. V. Nazarov, and L. M. K. Vandersypen, *Science* **318**, 1430 (2007).
 - [11] E. A. Laird, C. Barthel, E. I. Rashba, C. M. Marcus, M. P. Hanson, and A. C. Gossard, *Phys. Rev. Lett.* **99**, 246601 (2007).
 - [12] M. Pioro-Ladriere, T. Obata, Y. Tokura, Y. S. Shin, T. Kubo, K. Yoshida, T. Taniyama, and S. Tarucha, *Nature Phys.* **4**, 776 (2008).
 - [13] L. R. Schreiber, F. R. Braakman, T. Meunier, V. Calado, J. Danon, J. M. Taylor, W. Wegscheider, and L. M. K. Vandersypen, *Nat. Commun.* **2**, 556 (2011).
 - [14] M. Shafiei, K. C. Nowack, C. Reichl, W. Wegscheider, and L. M. K. Vandersypen, *Phys. Rev. Lett.* **110**, 107601 (2013).
 - [15] A. V. Khaetskii and Y. V. Nazarov, *Phys. Rev. B* **61**, 12639 (2000).
 - [16] A. V. Khaetskii and Y. V. Nazarov, *Phys. Rev. B* **64**, 125316 (2001).
 - [17] V. N. Golovach, A. Khaetskii, and D. Loss, *Phys. Rev. Lett.* **93**, 016601 (2004).
 - [18] D. V. Bulaev and D. Loss, *Phys. Rev. B* **71**, 205324 (2005).
 - [19] P. Stano and J. Fabian, *Phys. Rev. B* **72**, 155410 (2005).
 - [20] P. Stano and J. Fabian, *Phys. Rev. Lett.* **96**, 186602 (2006).
 - [21] S. Amasha, K. MacLean, I. P. Radu, D. M. Zumbühl, M. A. Kastner, M. P. Hanson, and A. C. Gossard, *Physical Review Letters* **100**, 046803 (2008).
 - [22] S. I. Erlingsson, Y. V. Nazarov, and V. I. Fal'ko, *Phys. Rev. B* **64**, 195306 (2001).
 - [23] S. I. Erlingsson and Y. V. Nazarov, *Phys. Rev. B* **66**, 155327 (2002).
 - [24] I. A. Merkulov, A. L. Efros, and M. Rosen, *Phys. Rev. B* **65**, 205309 (2002).
 - [25] A. C. Johnson, J. R. Petta, J. M. Taylor, A. Yacoby, M. D. Lukin, C. M. Marcus, M. P. Hanson, and A. C. Gossard, *Nature* **435**, 925 (2005).
 - [26] F. H. L. Koppens, J. A. Folk, J. M. Elzerman, R. Hanson, L. H. W. van Beveren, I. T. Vink, H. P. Tranitz, W. Wegscheider, L. P. Kouwenhoven, and L. M. K. Vandersypen, *Science* **309**, 1346 (2005).
 - [27] J. M. Taylor, J. R. Petta, A. C. Johnson, A. Yacoby, C. M. Marcus, and M. D. Lukin, *Phys. Rev. B* **76**, 035315 (2007).
 - [28] W. G. van der Wiel, S. De Franceschi, J. M. Elzerman, T. Fujisawa, S. Tarucha, and L. P. Kouwenhoven, *Rev. Mod. Phys.* **75**, 1 (2002).
 - [29] T. Hayashi, T. Fujisawa, H. D. Cheong, Y. H. Jeong, and Y. Hirayama, *Phys. Rev. Lett.* **91**, 226804 (2003).
 - [30] J. R. Petta, A. C. Johnson, C. M. Marcus, M. P. Hanson, and A. C. Gossard, *Phys. Rev. Lett.* **93**, 186802 (2004).
 - [31] J. Gorman, D. G. Hasko, and D. A. Williams, *Phys. Rev. Lett.* **95**, 090502 (2005).
 - [32] T. Fujisawa, T. H. Oosterkamp, W. G. van der Wiel, B. W. Broer, R. Aguado, S. Tarucha, and L. P. Kouwenhoven, *Science* **282**, 932 (1998).
 - [33] M. Raith, P. Stano, F. Baruffa, and J. Fabian, *Phys. Rev. Lett.* **108**, 246602 (2012).
 - [34] Y. Y. Wang and M. W. Wu, *Phys. Rev. B* **74**, 165312 (2006).
 - [35] M. Wang, Y. Yin, and M. W. Wu, *J. Appl. Phys.* **109**, 103713 (2011).
 - [36] J. Fabian and S. Das Sarma, *Physical Review Letters* **81**, 5624 (1998).
 - [37] M. Raith, P. Stano, and J. Fabian, *Phys. Rev. B* **83**, 195318 (2011).
 - [38] E. I. Rashba, *Sov. Phys. Solid State* **2**, 1109 (1960).
 - [39] Y. A. Bychkov and E. I. Rashba, *J. Phys. C* **17**, 6039 (1984).
 - [40] G. Dresselhaus, *Phys. Rev.* **100**, 580 (1955).
 - [41] Note that Ω_z implicitly includes the homogeneous part of the nuclear field.
 - [42] See Supplemental Material.
 - [43] J. M. Elzerman, R. Hanson, L. H. Willems van Beveren, B. Witkamp, L. M. K. Vandersypen, and L. P. Kouwenhoven, *Nature* **430**, 431 (2004).
 - [44] K. C. Nowack, M. Shafiei, M. Laforest, G. E. D. K. Prawiroatmodjo, L. R. Schreiber, C. Reichl, W. Wegscheider, and L. M. K. Vandersypen, *Science* **333**, 1269 (2011).
 - [45] G. Mahan, *Many-Particle Physics* (Plenum, 1990).
 - [46] T. Fujisawa, Y. Tokura, and Y. Hirayama, *Phys. Rev. B* **63**, 081304 (2001).
 - [47] J. R. Schrieffer and P. A. Wolff, *Physical Review* **149**, 491 (1966).
 - [48] C. H. Yang, A. Rossi, R. Ruskov, N. S. Lai, F. A. Mohiyaddin, S. Lee, C. Tahan, G. Klimeck, A. Morello, and A. S. Dzurak, arXiv:1302.0983v1 .

Supplemental Material: Simultaneous Spin-Charge Relaxation in Double Quantum Dots

V. Srinivasa,¹ K. C. Nowack,² M. Shafiei,² L. M. K. Vandersypen,² and J. M. Taylor¹

¹*Joint Quantum Institute, University of Maryland, College Park, MD 20742 and National Institute of Standards and Technology, Gaithersburg, MD 20899*

²*Kavli Institute of Nanoscience, TU Delft, Lorentzweg 1, 2628CJ Delft, the Netherlands*

I. SPIN RELAXATION RATE MEASUREMENT

The measurement illustrated in Fig. 1 of the main text is performed on a DQD formed by using Ti/Au surface gates to locally deplete a two-dimensional electron gas 90 nm below the surface of a GaAs/(Al,Ga)As heterostructure. Quantum point contacts (QPCs) on both sides of the DQD are used to detect the charge on each dot. We tune the DQD to contain a single electron (Fig. S1) and operate close to the degeneracy of $|L\rangle$ and $|R\rangle$. To set the electrochemical potentials in the left and right dot independently, combinations of voltages on two gates, one closer to the left dot and the other closer to the right dot, are tuned which compensate for capacitive cross-coupling. The tunnel coupling is tuned to be approximately $8 \mu\text{eV}$. Both the tunnel coupling and the conversion from applied gate voltage to change in detuning are determined from microwave spectroscopy [1]. An in-plane magnetic field $B_{\text{ext}} = 6.5 \text{ T}$ is applied to split the spin-up and spin-down energy of the electron by the Zeeman energy ($E_Z \approx 130 \mu\text{eV}$). The electron temperature is typically 250 mK [2].

II. COMPARISON OF DIRECT AND INDIRECT SPIN RELAXATION RATES

The relative contributions of the direct and indirect transitions described in the main text to the overall relaxation rate are characterized by the ratio Γ_e/Γ_b . An estimate of this ratio can be obtained by combining the dipole-dependent factors $\langle |d_b|^2 \rangle$ and $\langle |d_e|^2 \rangle$ given in Eqs. (8) and (9) of the main text with the corresponding energy-dependent factors $F(\Delta_b)$ and $F(\Delta_e)$, where $\Delta_b \approx \Omega_z$ and $\Delta_e \approx \Omega_z - \Delta$ are the associated energy gaps. To determine an approximate form for $F(\Delta_d)$, we consider the full expression obtained from Fermi's golden rule for the rate of decay induced by H_{ep} [Eq. (6) of the main text]. Defining $M_k \equiv e^{i\mathbf{k}\cdot\mathbf{r}}$, we obtain

$$\Gamma = \frac{2\pi}{\hbar} \sum_{\nu} \frac{V_0}{(2\pi)^3} \int k^2 dk \frac{\hbar}{2\rho_0 V_0 c_{\nu} k} (k^2 \beta_l^2 \delta_{\nu,l} + \Xi^2) I_{\text{ang}}(k) \delta(\varepsilon_{\text{ph}} - \Delta_d), \quad (\text{S1})$$

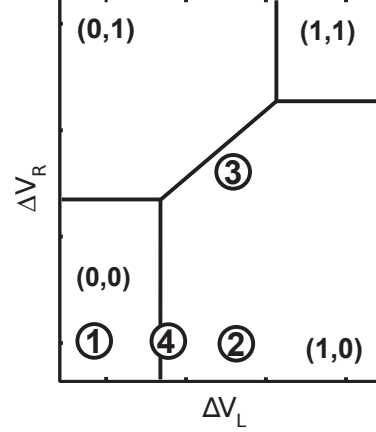


Figure S1: Schematic of the double quantum dot charge stability diagram associated with the steps in the measurement scheme of Fig. 1 in the main text. (n, m) represents a state with n electrons in the left dot and m electrons in the right dot. The charge configurations $(1, 0)$ and $(0, 1)$ correspond to the states $|L\rangle$ and $|R\rangle$, respectively, introduced in the main text. ΔV_L and ΔV_R represent the effective voltages applied to the left and right gates.

where we have converted the sum over \mathbf{k} to an integral, and

$$I_{\text{ang}}(k) = \int d\Omega |\langle f | M_k | i \rangle|^2 \quad (\text{S2})$$

is a momentum-space angular integral that is determined by the transition matrix element $\langle f | M_k | i \rangle$. In H_{ep} and Eq. (S1), a linear dispersion $\varepsilon_{\text{ph}} = \hbar c_{\nu} k$ for the phonon energies is assumed. The only factor in H_{ep} which depends on electronic degrees of freedom (specifically, on the position operator \mathbf{r} for the electron) is M_k , which can be expressed within the same two-level approximation used for H_d in Eqs. (1)-(4) of the main text. The form of M_k in the basis $\{|L\rangle, |R\rangle\}$ is given by

$$M_k = e^{-(k_y^2 + k_z^2)\sigma^2/2} \left[\cos\left(\frac{ak_z}{2}\right) \mathbf{1} - i \sin\left(\frac{ak_z}{2}\right) \sigma_z + e^{-a^2/8\sigma^2} \sigma_x \right], \quad (\text{S3})$$

where the term involving σ_x describes phonon-assisted tunneling between the left and right dots.

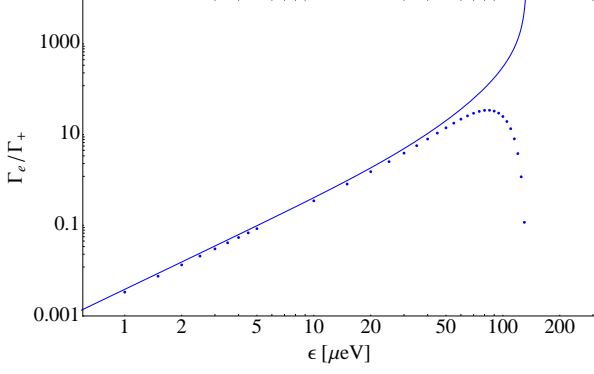


Figure S2: Comparison of the ratio Γ_e/Γ_b of the relaxation rates plotted in Fig. 2(c) of the main text (points) with the approximation in Eq. (S4) obtained using dipole matrix elements (line).

Retaining only the piezoelectric term (the dominant term for the parameters we choose [3]) in Eq. (S1), setting $\Delta_d = \varepsilon_{\text{ph}} = \hbar c_\nu k$, and noting that $I_{\text{ang}}(k) \sim 1/k^2$ in the limit of large k [4], which is the limit appropriate for the size of Δ_d at small detuning $|\epsilon|$ [see Fig. 2(a) of the main text], we find $F(\Delta_d) \sim \Delta_d^{-1}$. The ratio of the decay rates [averaged over the nuclear field distribution

in Eq. (7) of the main text] can then be estimated as

$$\begin{aligned} \frac{\langle \Gamma_e \rangle}{\langle \Gamma_b \rangle} &\sim \frac{\langle |d_e|^2 \rangle}{\langle |d_b|^2 \rangle} \left(\frac{\Omega_z - \Delta}{\Omega_z} \right)^{-1} \\ &= \left(\frac{\epsilon}{2t} \right)^2 \left(1 + \frac{\Delta}{\Omega_z} \right)^2 \left(1 - \frac{\Delta}{\Omega_z} \right)^{-1}. \end{aligned} \quad (\text{S4})$$

As $\epsilon \rightarrow 0$, $\Delta \rightarrow 2t \ll \Omega_z$ so that $\langle \Gamma_e \rangle / \langle \Gamma_b \rangle$ approaches $(\epsilon/2t)^2$. The estimated ratio in Eq. (S4) agrees well with the ratio Γ_e/Γ_b obtained from Fig. 2(c) of the main text for $|\epsilon| \ll \Omega_z$ (Fig. S2).

-
- [1] J. R. Petta, A. C. Johnson, C. M. Marcus, M. P. Hanson, and A. C. Gossard, Phys. Rev. Lett. **93**, 186802 (2004).
 - [2] K. C. Nowack, M. Shafiei, M. Laforest, G. E. D. K. Prawiroatmodjo, L. R. Schreiber, C. Reichl, W. Wegscheider, and L. M. K. Vandersypen, Science **333**, 1269 (2011).
 - [3] R. Hanson, L. P. Kouwenhoven, J. R. Petta, S. Tarucha, and L. M. K. Vandersypen, Rev. Mod. Phys. **79**, 1217 (2007).
 - [4] S. Vorojtsov, E. R. Mucciolo, and H. U. Baranger, Phys. Rev. B **71**, 205322 (2005).